

Article

Numerical Study on Heat Transfer Deterioration of Supercritical *n*-Decane in Horizontal Circular Tubes

Yanhong Wang, Sufen Li * and Ming Dong

School of Energy and Power Engineering, Dalian University of Technology, Dalian 116024, China; E-Mails: wangyh.526@163.com (Y.W.); dongming@dlut.edu.cn (M.D.)

* Author to whom correspondence should be addressed; E-Mail: lisuf@dlut.edu.cn; Tel./Fax: +86-411-8470-8540.

External Editor: Vasily Novozhilov

Received: 10 September 2014; in revised form: 14 October 2014 / Accepted: 3 November 2014 / Published: 18 November 2014

Abstract: In order to obtain a deeper understanding of the regenerative cooling process of scramjet engines, in this paper, a numerical investigation on the supercritical convective heat transfer of *n*-decane in horizontal circular tubes was conducted, based on a complete set of conservation equations and the Renormalization group (RNG) k - ϵ turbulence model with enhanced wall treatment. The present study mainly focuses on the heat transfer deterioration (HTD) phenomenon, including the mechanism and critical conditions for the onset of HTD. Moreover, the applicability of some conventional heat transfer empirical correlations was analyzed and compared, thus providing guidance for the Nusselt number predictions in the cooling channels. Results indicate that under the compositive conditions of low pressure and high heat flux, two types of HTD phenomena could occur when the wall and bulk fluid temperatures are near the pseudo-critical temperature, owing to the abnormal distributions of near-wall turbulent kinetic energy and radial velocity, respectively. Increasing the pressure would effectively alleviate and eliminate the HTD. A comparison of numerical results with those obtained with different empirical expressions shows that the Bae-Kim expression provides the best agreement, especially when HTD occurs. Furthermore, a new correction for critical heat flux of HTD has been successfully developed.

Keywords: supercritical pressure; *n*-decane; convective heat transfer; heat transfer deterioration; critical condition; numerical study

1. Introduction

The regenerative cooling of hydrocarbon fuels has been widely considered as one of the most practical and effective thermal protection methods for scramjet engines [1]. In a regenerative cooling system, before injection into the combustion chamber, the fuel acts as a coolant and flows through the cooling channels, carrying heat away from the high temperature combustor wall, which can effectively improve both of the engine performance and energy utilization [2]. The operational pressure (p) of fuel in the cooling channels is generally above its critical pressure (p_c). Under a supercritical pressure, the thermo-physical properties of fuel, such as density, specific heat capacity, thermal conductivity and dynamic viscosity, change dramatically with temperature, especially when its temperature is near the pseudo-critical temperature (T_{pc} , corresponds to the maximum specific heat capacity) and the pressure is close enough to the critical pressure [3], and this leads to complex flow and heat transfer phenomena.

The existing investigations on convective heat transfer of supercritical fluids have been focused mainly on carbon dioxide [4] and water [5], and have obtained great achievements in the research on heat transfer deterioration (HTD) phenomena [6–10]. Jiang *et al.* [6] studied experimentally the flow and heat transfer characteristics of carbon dioxide in vertical circular tubes at supercritical pressures. They concluded that the HTD was due to the flow laminarization near the wall, and occurred only in upward flow when the buoyancy effect was large enough. Wen *et al.* [7] and Koshizuka *et al.* [8] investigated numerically the HTD phenomena of supercritical water in circular channels, and found that these HTDs were mainly caused by strong buoyancy forces, but with different mechanisms. Wen *et al.* [7] argued that the buoyancy force caused the deformation of velocity profile and impairment of turbulent production, leading to the HTD with low bulk fluid temperature. Besides, the second HTD phenomenon may occur in the high bulk fluid temperature region if the full recovery of heat transfer after the first HTD was achieved with the help of a quite strong buoyancy force. Koshizuka *et al.* [8] maintained that the HTD occurred due to two mechanisms depending on the mass flux. The flow velocity was accelerated and the turbulent kinetic energy was reduced near the wall due to the buoyancy force, resulting in the HTD at low mass fluxes, while the increasing local viscosity near the wall made the Prandtl number smaller and the viscous sub-layer thicker, which finally led to the HTD at large mass fluxes. Another important reason for the HTD of supercritical fluids is the thermal acceleration. Related HTD phenomena have been observed in experimental research on supercritical carbon dioxide by Kim *et al.* [9], and supercritical water by Zhang *et al.* [10].

So far, very few studies about HTD of supercritical hydrocarbon fuels have been reported in the open literature [11–18]. Wang *et al.* [11] and Hua *et al.* [12] performed a numerical study of supercritical turbulent heat transfer of methane [11] and *n*-heptane [12] inside a horizontal miniature tube, respectively. Results indicated that the heat transfer performances of both were good under a higher pressure, but the HTD could occur once the wall temperature reached the pseudo-critical temperature due to a rapid decrease in the volumetric heat capacity when the pressure was close to the corresponding critical pressure. Urbano *et al.* [13–15], Zhou *et al.* [16] carried out operational parametric numerical studies of the HTD in supercritical light hydrocarbon fuels, including the methane [13–15] and pentane [16], in horizontal circular channels. Moreover, critical conditions for the occurrence of HTD were developed [15,16]. Hitch and Karpuk [17] studied experimentally the supercritical convective heat transfer of JP-7 aviation kerosene in vertical circular tubes, and they

observed deteriorated heat transfer along with significant temperature and pressure oscillations, when the reduced pressure (p/p_c) was below 1.5 and the wall temperature was over the pseudo-critical temperature. Liu *et al.* [18] also conducted similar experimental studies, and emphatically analyzed the heat transfer and pressure drop characteristics of another type of kerosene inside horizontal circular channels, and concluded that at near-critical pressures, HTD would occur as the film temperature approached the pseudo-critical temperature, accompanied with abnormal phenomena of flow instability and pressure drop deduction, during the corresponding process. As the bulk fluid temperature increased to above the pseudo-critical temperature, the heat transfer and flow stability were regained. Although a certain number of experimental and numerical studies have been conducted to examine the HTD phenomena in supercritical hydrocarbon fuels, more fundamental investigations, especially of the mechanism and critical conditions for the onset of HTD, still need to be further performed.

In this paper, a numerical investigation on supercritical convective heat transfer of a typical hydrocarbon fuel, *n*-decane, flowing through horizontal circular tubes has been conducted with the commercial software Fluent 6.3. The present study will focus on the fundamental understanding of the HTD phenomena, including the mechanism and critical conditions for the onset of HTD, and the applicability of several conventional empirical heat transfer expressions, with the expectation of providing some useful reference data for the design and optimization of the regenerative cooling systems of scramjet engines.

2. Models and Numerical Methods

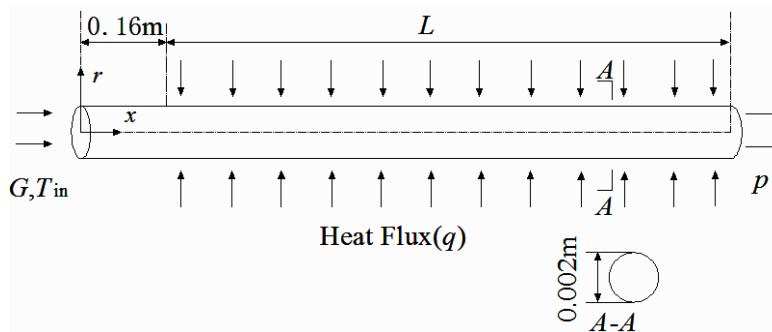
2.1. Physical Model and Boundary Conditions

A sketch of the physical model and the applied boundary conditions is shown in Figure 1. The inner diameter of the tube (d) is 0.002 m. The complete computational domain covers the unheated and heated sections. The length of the unheated section is 0.16 m, so that the flow into the heated section is fully developed. A uniform heat flux is imposed on the tube wall in the heated section, the length of which varies depending on different heat fluxes. For a specific heat flux, the length of the heated section is determined according to the heat balance, *i.e.*, the heating quantity through the wall is equal to the inlet-outlet fluid enthalpy (H) increase. Taking the constant mass flux $G = 1200 \text{ kg}/(\text{m}^2 \cdot \text{s})$ as an example, the length of the heated section (L) may be 4.2, 3.0, 2.1, 1.7, 1.4 or 1.1 m, corresponding to the tubes with different heat fluxes (q) of 200, 300, 400, 500, 600 and 700 kW/m^2 , respectively. The inlet and outlet boundary conditions of the computational domain are specified as mass flux inlet and pressure outlet, respectively. The same inlet temperature $T_{\text{in}} = 340 \text{ K}$ is assigned for all the simulations, and all the outlet bulk fluid temperatures are about 820 K, so as to ensure the *n*-decane ($p_c = 2.1 \text{ MPa}$, $T_c = 618 \text{ K}$ [19]) experiences the entire process from the over-pressure liquid state to the supercritical state. The range of the outlet pressure is 3–5 MPa.

The present study only discusses the convective heat transfer without obvious thermal cracking, so the calculation data analyzed here are limited in the tube section where the wall temperature is below 870 K [19]. The gravity effects are neglected because the ratio between the real Grashof number (Gr_q) and the threshold Grashof number (Gr_{th}) is less than 4×10^{-3} based on the entrance parameters, and

thus it is similar to a 2D axisymmetric problem. In addition, a certain length are retained in both ends of the heated section to further avoid the effects of inflow and outflow boundary conditions on the numerical results, only the flow and heat transfer characteristics in the bulk fluid temperature range of 425–770 K are concerned.

Figure 1. Sketch map of the physical model and the applied boundary conditions.



2.2. Governing Equations

The present numerical study is based on a complete set of conservation equations of mass, momentum and energy in cylindrical coordinates, as presented in the following forms:

Mass conservation:

$$\frac{1}{r} \left\{ \frac{\partial}{\partial x} (r\rho u_x) + \frac{\partial}{\partial r} (r\rho u_r) \right\} = 0 \tag{1}$$

U-momentum conservation:

$$\frac{1}{r} \left\{ \frac{\partial}{\partial x} (r\rho u_x^2) + \frac{\partial}{\partial r} (r\rho u_r u_x) \right\} = -\frac{\partial p}{\partial x} + \frac{1}{r} \left\{ 2 \frac{\partial}{\partial x} \left[r\mu_e \left(\frac{\partial u_x}{\partial x} \right) \right] + \frac{\partial}{\partial r} \left[r\mu_e \left(\frac{\partial u_x}{\partial r} + \frac{\partial u_r}{\partial x} \right) \right] \right\} \tag{2}$$

V-momentum conservation:

$$\frac{1}{r} \left\{ \frac{\partial}{\partial x} (r\rho u_x u_r) + \frac{\partial}{\partial r} (r\rho u_r^2) \right\} = -\frac{\partial p}{\partial r} + \frac{1}{r} \left\{ \frac{\partial}{\partial x} \left[r\mu_e \left(\frac{\partial u_r}{\partial x} + \frac{\partial u_x}{\partial r} \right) \right] + 2 \frac{\partial}{\partial r} \left[r\mu_e \left(\frac{\partial u_r}{\partial r} \right) \right] \right\} - 2 \frac{\mu_e u_r}{r^2} \tag{3}$$

Energy conservation:

$$\frac{1}{r} \left\{ \frac{\partial}{\partial x} (r\rho u_x h) + \frac{\partial}{\partial r} (r\rho u_r h) \right\} = \frac{1}{r} \left\{ \frac{\partial}{\partial x} \left[r \left(\frac{\mu}{Pr} + \frac{\mu_T}{\sigma_T} \right) \frac{\partial h}{\partial x} \right] + \frac{\partial}{\partial r} \left[r \left(\frac{\mu}{Pr} + \frac{\mu_T}{\sigma_T} \right) \frac{\partial h}{\partial r} \right] \right\} \tag{4}$$

The Renormalization group (RNG) $k-\epsilon$ turbulence model with enhanced wall treatment can better predict the convective heat transfer of supercritical fluids [20], which are employed in this study. The RNG $k-\epsilon$ turbulent equations are given as follows:

Turbulent kinetic energy:

$$\left\{ \frac{\partial}{\partial x} (\rho u_x k) + \frac{1}{r} \frac{\partial}{\partial r} (r\rho u_r k) \right\} = \frac{\partial}{\partial x} \left[\left(\mu + \frac{\mu_T}{\sigma_k} \right) \frac{\partial k}{\partial x} \right] + \frac{1}{r} \frac{\partial}{\partial r} \left[r \left(\mu + \frac{\mu_T}{\sigma_k} \right) \frac{\partial k}{\partial r} \right] + G_k - \rho\epsilon \tag{5}$$

Turbulence dissipation rate:

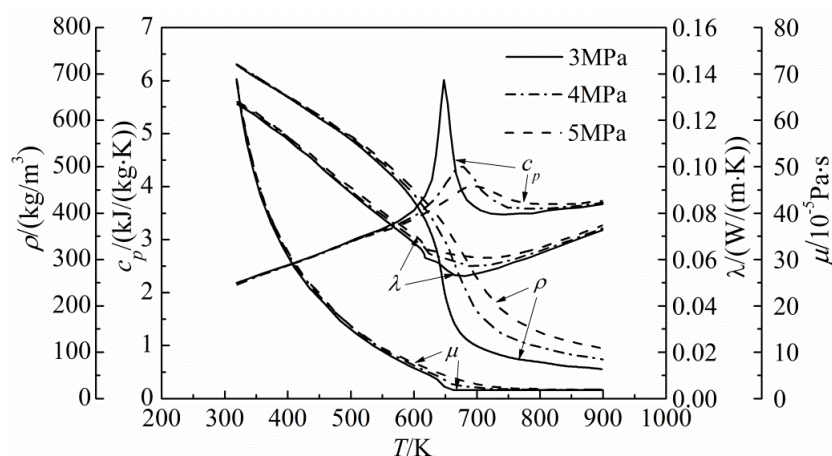
$$\left\{ \frac{\partial}{\partial x} (\rho u_x \varepsilon) + \frac{1}{r} \frac{\partial}{\partial r} (r \rho u_r \varepsilon) \right\} = \frac{\partial}{\partial x} \left[\left(\mu + \frac{\mu_t}{\sigma_\varepsilon} \right) \frac{\partial \varepsilon}{\partial x} \right] + \frac{1}{r} \frac{\partial}{\partial r} \left[r \left(\mu + \frac{\mu_t}{\sigma_\varepsilon} \right) \frac{\partial \varepsilon}{\partial r} \right] + C_{1\varepsilon} G_k \frac{\varepsilon}{k} + C_{2\varepsilon} \rho \frac{\varepsilon^2}{k} - R_\varepsilon \quad (6)$$

The relevant variables in Equations (1)–(6) can be found in [7].

2.3. Thermo-Physical Properties

The thermo-physical properties of *n*-decane, including the density (ρ), specific heat capacity (c_p), thermal conductivity (λ) and dynamic viscosity (μ), as a function of temperature and pressure, are all computed by the National Institute of Standards and Technology (NIST) Supertrapp software [20], as shown in Figure 2.

Figure 2. Thermo-physical properties of *n*-decane at supercritical pressures.



2.4. Grids and Numerical Methods

Structured body-fitted grids are used here. In order to achieve the required precision for the computational data, the grids are refined in the near-wall region. Furthermore, there should be 10 grids within the viscosity-dominant near-wall region (*i.e.*, $y^+ \leq 5$), and the first grid node adjacent to the wall is constructed to satisfy the requirement of $y^+ \leq 1$.

The double-precision pressure-based solver is adopted to solve the governing equations. A finite-volume method is used for the discretization of the governing equations, the convection terms in the governing equations are discretized with the second-order upwind scheme, and the second-order central scheme is used to discretize the diffusion terms. The pressure-velocity coupling is implemented by the SIMPLEC algorithm. The implicit Gauss-Seidel iteration is used to handle the time advancing. The absolute convergence criterion for continuity is that the residual is less than 10^{-5} , and the residuals of other governing equations are set to be less than 10^{-7} .

2.5. Grid-Independence Analysis and Numerical Methods Validation

Before performing detailed numerical studies, the grid-independence analysis and numerical methods validation are conducted to ensure the accuracy of the present numerical calculations. Taking the tube

with a total length of 1.26 m as an example, three different grid systems (cross-sectional \times axial) of 1545×250 , 3056×500 and 6124×1000 are selected, and the calculated results are compared with the available experimental data obtained by Liu *et al.* ($p = 3$ MPa, $G = 708$ kg/(m²·s), $q = 351$ kW/m², $T_{in} = 423$ K, $d = 2$ mm, downward flow) [21]. Figure 3 shows variations of the wall temperature and heat transfer coefficient (HTC) with reduced axial length. The HTC is defined as:

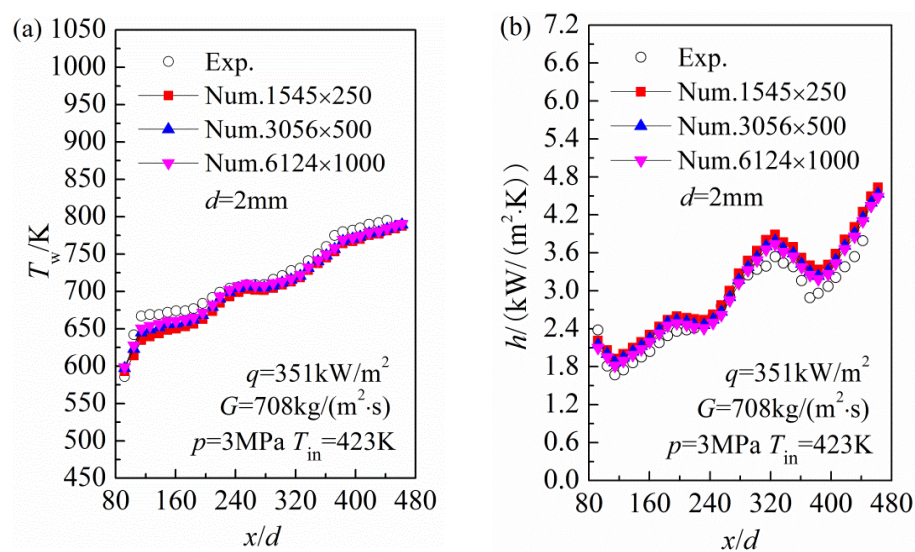
$$h = q / (T_w - T_b) \quad (7)$$

where T_b is the bulk fluid temperature (K) calculated as:

$$T_b = \int_A \rho u c_p T dA / \int_A \rho u c_p dA \quad (8)$$

where u is the velocity (m/s); A is the cross-section area (m²); Subscripts “w” and “b” represent wall and bulk fluid, respectively.

Figure 3. Grid-independence analysis and numerical methods validation: (a) wall temperature; and (b) heat transfer coefficient (HTC).



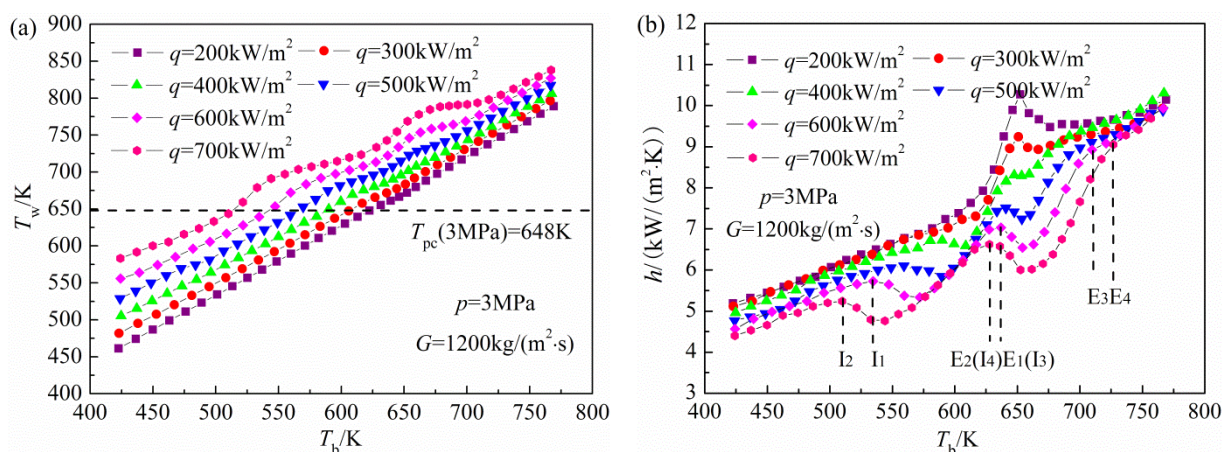
As shown in Figure 3, increasing the meshes from 3056×500 to 6124×1000 causes less than 1.6% and 2.1% relative numerical errors in terms of wall temperature and HTC, respectively; while by decreasing the meshes from 3056×500 to 1545×250 , the relative numerical errors are generally 3.5% and 4.7%, respectively. This indicates that a grid system with 3056 and 500 meshes in the cross-sectional and axial directions, respectively, is sufficient, and thus be used in the follow numerical calculations. In addition, it can be seen from Figure 3 that the calculated wall temperature and HTC with the 3056×500 grid system show excellent agreement with the experimental data, as the relative errors are within 5.2% and 6.8%, respectively. Particularly the RNG k - ϵ turbulence model with enhanced wall treatment is applicable for the wall temperature oscillation and HTD predictions, indicating that the models and numerical methods used in this study are reasonable and reliable, and the calculation results have good precision. For other tubes, the grid distributions in the cross-sectional direction remains the same, while the meshes in the axial direction increases in direct proportion to its length, thus the grid systems of 3056×620 (1.56 m), 3056×740 (1.86 m), 3056×905 (2.26 m), 3056×1260 (3.16 m) and 3056×1740 (4.36 m) are selected, respectively.

3. Results and Discussion

3.1. Effects of Heat Flux and Pressure on the Heat Transfer

The effects of the heat flux and pressure on the supercritical convective heat transfer of *n*-decane are studied in this section. The mass flux is $1200 \text{ kg}/(\text{m}^2 \cdot \text{s})$, the heat flux ranges from 200 to $700 \text{ kW}/\text{m}^2$, while the outlet pressures are 3 and 5 MPa, respectively. Variations of the wall temperature and HTC with bulk fluid temperature at a pressure of 3 MPa are presented in Figure 4.

Figure 4. Variations of the wall temperature and HTC with bulk fluid temperature at a pressure of 3 MPa: (a) wall temperature; and (b) HTC.



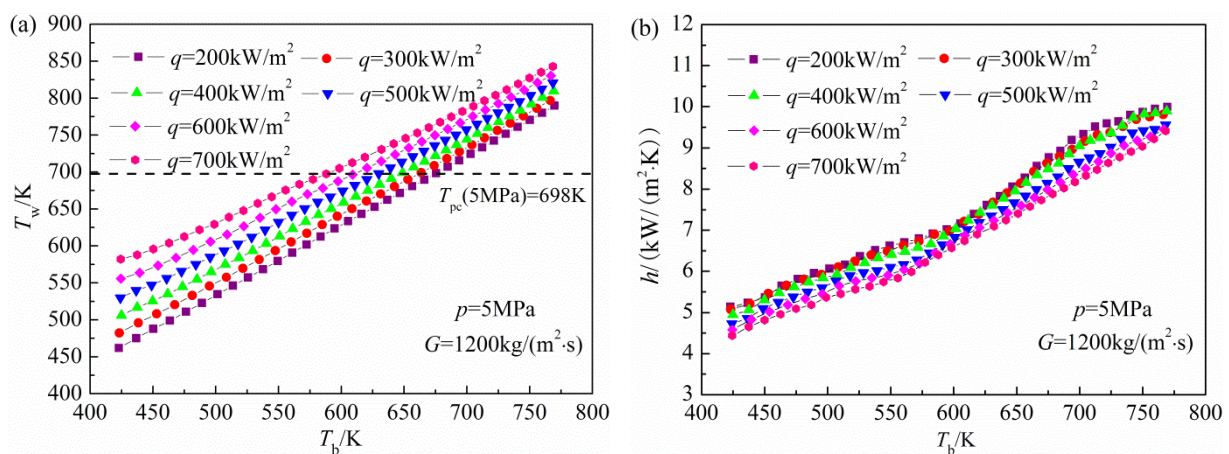
As shown in Figure 4a, under low heat fluxes, *i.e.*, 200 and $300 \text{ kW}/\text{m}^2$, the wall temperature increases linearly with the increase of bulk fluid temperature. Under moderate heat fluxes of 400 and $500 \text{ kW}/\text{m}^2$, an interesting phenomenon is discovered in that a slight oscillation in the wall temperature occurs once it exceeds the corresponding pseudo-critical temperature. As the heat flux further increases further, *i.e.*, 600 and $700 \text{ kW}/\text{m}^2$, the wall temperature oscillation becomes more intense and two obvious peaks appear, indicating complex flow and heat transfer phenomena, which can be further explained by variation in the HTC.

As shown in Figure 4b, under low heat fluxes of 200 and $300 \text{ kW}/\text{m}^2$, the total heat transfer process can be divided into three typical regions, and this is closely related to the variations of bulk fluid thermo-physical properties: (1) $T_b \leq 614 \text{ K}$. The specific heat capacity rises with the increasing bulk fluid temperature, indicating that the fluid can carry away more heat from the tube wall. On the other hand, the axial velocity increases quickly owing to a continuous decrease in the density and dynamic viscosity, both of which lead to a linear increase of the HTC along the flow direction; (2) $614 \text{ K} \leq T_b \leq 686 \text{ K}$. When the bulk fluid temperature approaches to its pseudo-critical temperature, the thermo-physical properties begin to change greatly, as a consequence, comprehensive effects of the specific heat capacity, density and dynamic viscosity lead to a significantly enhanced heat transfer. Then, the bulk fluid temperature exceeds the pseudo-critical temperature, and a rapid decrease of the specific heat capacity causes a slight deterioration in heat transfer; (3) $T_b \geq 686 \text{ K}$. The density, specific heat capacity and dynamic viscosity change slightly, and merely the variation of the thermal conductivity is beneficial to enhance the heat transfer, so the HTC gradually increases as the bulk fluid

temperature increases. Under these operational conditions, the HTC and bulk fluid specific heat capacity have similar variation tendencies. Obviously, the specific heat capacity is the most important factor influencing the heat transfer performance, and a HTC peak appears due to the bulk fluid temperature in the large specific heat capacity region. As the heat flux increases, because of the wall temperature oscillation, the variation of the HTC along the flow direction becomes more complicated, the HTD occurs in both the low and high bulk temperature regions. The same phenomenon has also been observed in an experimental study of the convective heat transfer of *n*-decane under supercritical pressures [21], as mentioned above. The degree of deteriorated heat transfer deepens gradually with increasing heat flux, featuring a larger corresponding bulk fluid temperature range. Mechanisms of the HTD will be discussed in detail in the following sections, taking $q = 200, 600, 700 \text{ kW/m}^2$ in Figure 4 as examples.

Figure 5 presents variations of the wall temperature and HTC along the tube axial direction at a high pressure of 5 MPa. As clearly depicted in Figure 5a, the wall temperature increases linearly with the increasing bulk fluid temperature for every heat flux, and no wall temperature oscillation occurs, indicating a good heat transfer performance at higher pressures. This fact is further validated by the variation of HTC, as illustrated in Figure 5b.

Figure 5. Variations of the wall temperature and HTC with bulk fluid temperature at a pressure of 5 MPa: (a) wall temperature; (b) HTC.



Furthermore, the HTC and bulk fluid specific heat capacity show a consistent variation trend along the flow direction, similar to those two low heat flux operational conditions when $p = 3 \text{ MPa}$, as mentioned above. It can be concluded that the HTD of supercritical *n*-decane is closely related to the operational pressure, and only appears in a relatively smaller near-critical pressure range. It can be expected that the critical heat flux of HTD will also increase accordingly with increasing pressure. The critical conditions for the onset of HTD will be analyzed below.

Since the HTD becomes more serious with the increase in heat flux, it is necessary to define a boundary so as to determine when the deterioration is safe, and when the deterioration is unsafe. For this purpose, Shiralkar *et al.* [22] stated that the HTD will do damage to the system safety operation, when the following conditions are satisfied:

$$Nu_{D-B}/Nu > 2 \quad (9)$$

where Nu_{D-B} obtained from the Dittus–Boelter correlation, which is given as follows:

$$Nu_{D-B} = 0.023 Re_b^{0.8} Pr_b^{0.4} \quad (10)$$

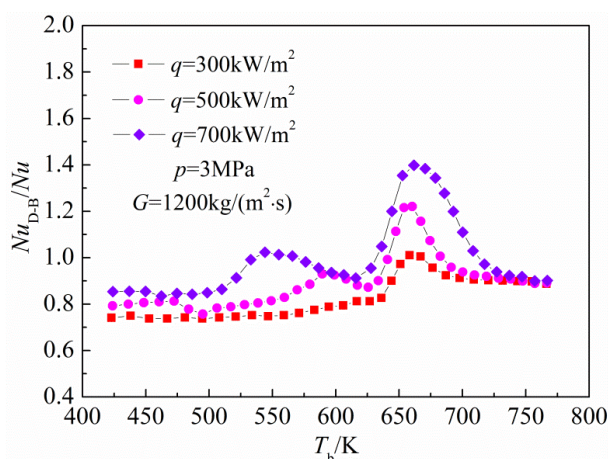
where Re_b and Pr_b are the Reynolds number and Prandtl number, respectively, based on properties at the bulk fluid temperature.

The Nusselt number is defined as:

$$Nu = hd/\lambda_b \quad (11)$$

Figure 6 presents variations of Nu_{D-B}/Nu with bulk fluid temperature at a pressure of 3 MPa. As shown in Figure 6, Nu_{D-B}/Nu increases with the increase of heat flux, and in general, the maximum value of Nu_{D-B}/Nu corresponds to the same position of the minimum HTC point. When the heat flux is 700 kW/m², the maximum value of Nu_{D-B}/Nu is about 1.4, lower than the critical value proposed by Shiralkar *et al.* [22]. As the heat flux further increases, significant thermal cracking will occur in the large specific heat capacity region because the wall temperature generally exceeds 870 K. The thermal cracking is an endothermic reaction, can absorb heat through the chemical heat sink, and as a result enhance the heat transfer [23]. Therefore, it can be concluded that the HTD will not cause serious harm to the cooling system under these operational conditions. In addition, Figure 6 also indicates that the Dittus–Boelter expression is no longer applicable for the heat transfer predictions.

Figure 6. Variations of Nu_{D-B}/Nu with bulk fluid temperature at a pressure of 3 MPa.



In order to better predict the convective heat transfer of *n*-decane under supercritical pressures, particularly the HTD phenomena, the applicability of several conventional empirical correlations are verified. Comparisons of the Nusselt number from both the present numerical calculations and the empirical expressions proposed by Bae-Kim [24], Gnielinski [11], Sieder-Tate [25], Bishop *et al.* [26], Mccarthy-Wolf [27], Taylor [27], Giovanetti *et al.* [28], are shown in Figures 7 and 8. The details of these correlations are in Table 1.

The Nusselt number from both the present numerical calculations (Nu_{cal}) and the empirical expressions (Nu_{emp}) at a pressure of 3 MPa are compared in Figure 7. As shown in Figure 7, at a low heat flux of 300 kW/m², the Nusselt number obtained from these seven expressions are in very good agreement with our present numerical results, all of the relative errors are generally within 25%.

When the heat flux is at a high level, *i.e.*, 700 kW/m², the Bae-Kim expression still has higher precision, and the relative error is less than 20%, meeting the accuracy requirements for engineering calculations. By contrast, the other expressions incur relatively large prediction deviations from the present numerical results, because they cannot predict the HTD phenomena. The maximum relative errors generally reaches around 40%, indicating that these expressions are invalid for heat transfer predictions of supercritical *n*-decane under high heat fluxes.

Figure 8 compares the Nusselt number from the numerical calculations and the seven empirical expressions at a pressure of 5 MPa. As shown in Figure 8, under a higher pressure, the HTD phenomena disappear due to the gentle thermal properties variations. Consequently, all these expressions have good applicability, the relative errors at two different heat fluxes are generally within 25%. Especially the Bae-Kim expression, the relative errors with the numerical results are less than 10%, indicating the best prediction performance.

Figure 7. Comparisons of the Nusselt number from the present numerical calculations and the empirical expressions under a pressure of 3 MPa: (a) $q = 300 \text{ kW/m}^2$; and (b) $q = 700 \text{ kW/m}^2$.

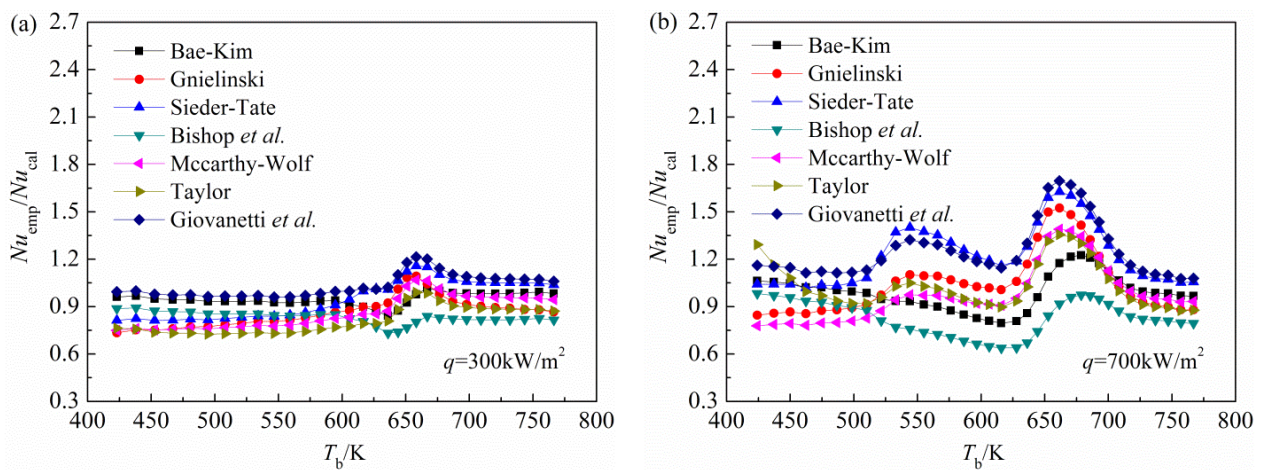


Figure 8. Comparisons of the Nusselt number from the present numerical calculations and the empirical expressions under a pressure of 5 MPa: (a) $q = 300 \text{ kW/m}^2$; and (b) $q = 700 \text{ kW/m}^2$.

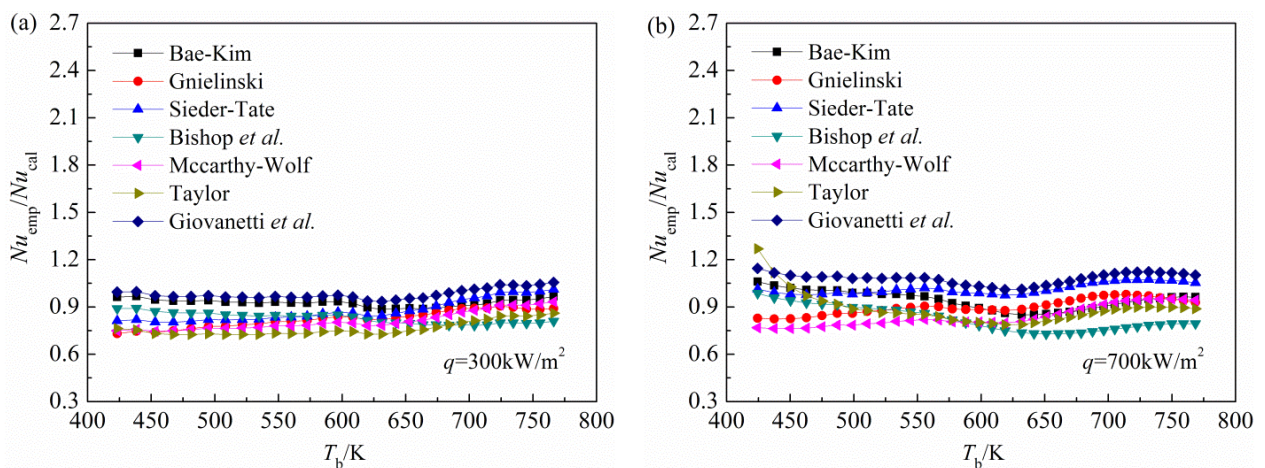


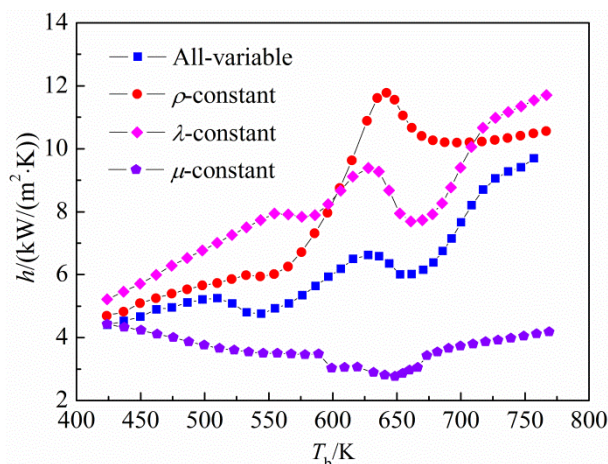
Table 1. Conventional convective heat transfer empirical correlations of supercritical fluids.

Author	Correlation	Fluid
Bae-Kim [24]	$Nu = 0.021 Re_b^{0.82} Pr_b^{0.5} (\rho_w / \rho_b)^{0.3} (\bar{c}_p / c_{pb})^n$ <p>where,</p> $n = \begin{cases} 0.4; T_b < T_w \leq T_{pc} \text{ or } 1.2T_{pc} \leq T_b < T_w \\ 0.4 + 0.2(T_w/T_{pc} - 1); T_b \leq T_{pc} < T_w \\ 0.4 + 0.2(T_w/T_{pc} - 1)[1 - 5(T_b/T_{pc} - 1)]; \\ T_{pc} < T_b \leq 1.2T_{pc} \text{ and } T_b < T_w \end{cases}$ $\bar{c}_p = \frac{H_w - H_b}{T_w - T_b}$	CO ₂
Gnielinski [11]	$Nu = \frac{(f/8)(Re_b - 1000)Pr_b}{1 + 12.7(f/8)^{0.5}(Pr_b^{2/3} - 1)}$ <p>where,</p> $f = (0.79 \ln(Re_b) - 1.64)^{-2}$	H ₂ O, CO ₂
Sieder-Tate [25]	$Nu = 0.027 Re_b^{4/5} Pr_b^{1/3} (\mu_b / \mu_w)^{0.14}$	H ₂ O, CO ₂
Bishop <i>et al.</i> [26]	$Nu = 0.0069 Re_b^{0.9} Pr_b^{0.66} (\rho_w / \rho_b)^{0.43} (\bar{c}_p / c_{pb})^{0.66} [1 + 2.4 d/x_L],$ <p>where x_L is the distance from the initial point of heating, m.</p>	H ₂ O
Mccarthy-Wolf [27]	$Nu = 0.025 Re_b^{0.8} Pr_b^{0.4} (T_b / T_w)^{0.55}$	H ₂
Taylor [27]	$Nu = 0.023 Re_b^{0.8} Pr_b^{0.4} (T_b / T_w)^{(0.57 - 1.59d/x_L)}$	H ₂
Giovanetti <i>et al.</i> [28]	$Nu = 0.044 Re_b^{0.76} Pr_b^{0.4} (1 + 2d/x_L)$	RP-1

In summary, the Bae-Kim expression, which has higher prediction accuracy when the HTD occurs, can be better used for supercritical heat transfer predictions of *n*-decane.

3.2. Mechanisms of the HTD

As described above, the specific heat capacity plays a dominant role in the heat transfer process of non-HTD operational conditions, indicating that it almost makes no contribution to the HTD phenomena. The influence of other fluid properties, *i.e.*, density, thermal conductivity and dynamic viscosity, on HTD are also investigated by setting one of these parameters as a constant (equal to the value corresponding to 425 K), while the others are still as a function of temperature in each calculation. The results are shown in Figure 9. As depicted in Figure 9, keeping the density constant, the HTD phenomena basically disappear; while keeping the thermal conductivity or dynamic viscosity constant, two types of HTD phenomena still exist. Consequently, it can be concluded that the occurrence of HTD closely relates to the dramatic changes of density with temperature. However, constant treatment is taken on the thermal conductivity or dynamic viscosity, the HTC shows a significantly increasing or decreasing tendency, which manifests that the variations of thermal conductivity and dynamic viscosity can worsen and enhance the heat transfer, respectively.

Figure 9. Effects of the thermo-physical properties on HTD under heat flux of 700 kW/m².

The previous studies on convective heat transfer of supercritical fluids in vertical circular tubes indicated that the HTD phenomena were closely related to the abnormal variations of turbulent kinetic energy near the wall [6–10]. To illustrate the relationship between the two, Figure 10 presents the distributions of near-wall ($r/R = 0.95$) turbulent kinetic energy (k) along the tube axial direction at three different heat fluxes. Where I_i , E_i ($i = 1-4$) are the corresponding tube cross-sections of the initial point of deteriorated heat transfer and the ending point of heat transfer recovered, respectively, as clearly depicted in Figure 4b. As shown in Figure 10, under a low heat flux of 200 kW/m², there is no abnormal distribution of the turbulent kinetic energy near the wall, and which increases monotonically along the flow direction. Under high heat fluxes of 600 and 700 kW/m², the near-wall turbulent kinetic energy first decreases and then increases along the tube axial direction, corresponding to the deteriorated heat transfer and heat transfer recovered in the low bulk fluid temperature region. This phenomenon indicates that the flow in the near-wall region has already transited from turbulent-like to laminar-like. The flow laminarization near the wall was generally caused by the strong buoyancy force in upward flow or thermal acceleration in downward flow [6–10], but for horizontal channels, so far, it has not yet been a consistent conclusion. During the related heat transfer process, *i.e.*, I_i – E_i ($i = 1,2$), it can be found from Figure 4a that the wall temperature is slightly higher than the pseudo-critical temperature, thus the fluid temperature in the near-wall region is close to the pseudo-critical temperature. Therefore, it can be considered that the near-wall fluid is subjected to a fluid acceleration effect due to large drops of the density with temperature, and thus the turbulent heat transfer near the wall is significantly suppressed [29], which resulting in the occurrence of HTD.

Figure 11 further presents variations of the wall shear stress (τ_w) with bulk fluid temperature. As shown in Figure 11, the wall shear stress and near-wall turbulent kinetic energy show a similar variation trend corresponding to the deteriorated heat transfer and heat transfer recovered in the low bulk fluid temperature region. This means that the frictional resistance has been subjected to a certain extent to weakening during the related heat transfer process. Clearly, this phenomenon is caused by the flow acceleration near the wall. As the wall temperature increases, the pseudo-critical point gradually moves away from the wall, the near-wall turbulent kinetic energy starts to slowly recover due to weakening of the flow acceleration, and thus the heat transfer is improved.

Figure 10. Variations of the near-wall turbulent kinetic energy with bulk fluid temperature under different heat fluxes.

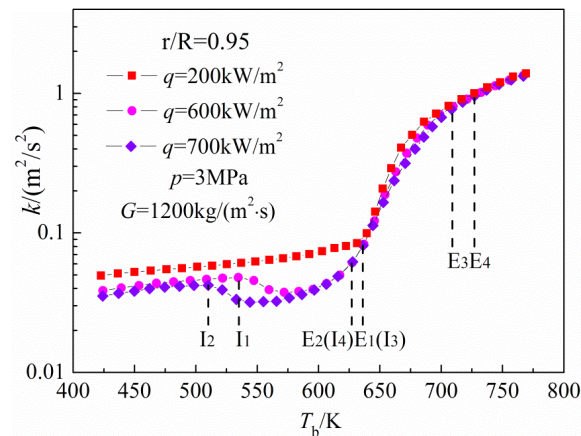
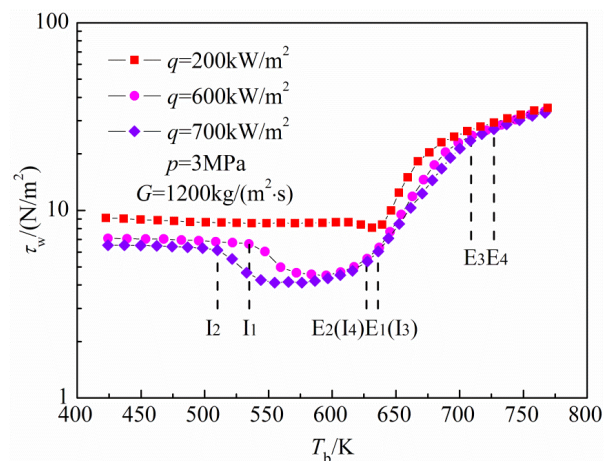


Figure 11. Variations of the wall shear stress with bulk fluid temperature under different heat fluxes.



In addition, Figures 10 and 11 also show that the mechanism of HTD in the high bulk fluid temperature region is very different from that of the low bulk fluid temperature region. It can be seen from Figure 4b that this type of HTD occurs when the bulk fluid temperature is in the vicinity of the pseudo-critical temperature. For this type of HTD, there has not yet been a clear mechanism analysis. For further explanation of this phenomenon, Figure 12 presents variations of the averaged radial velocity (u_{r-ave} , positive toward the wall) with bulk fluid temperature at three different heat fluxes, as mentioned above. As shown in Figure 12, under a low heat flux of 200 kW/m², the HTD does not appear and the averaged radial velocity is close to zero during the entire heat transfer process. As the heat flux increases, *i.e.*, 600 and 700 kW/m², the averaged radial velocity shows a larger variation, and two obvious waveforms, first negative and then positive, are observed corresponding to the deteriorated heat transfer and heat transfer recovered in the high bulk fluid temperature region. This phenomenon indicates that this HTD is necessarily linked with the abnormal distribution of radial velocity. Meng *et al.* [11,12] considered that the radial velocity oscillation had a negative impact on the heat transfer, and would lead to HTD and a slight oscillation of HTC, but its action mechanism on HTD has not yet received a detailed explanation.

Figure 12. Variations of the averaged radial velocity with bulk fluid temperature under different heat fluxes.

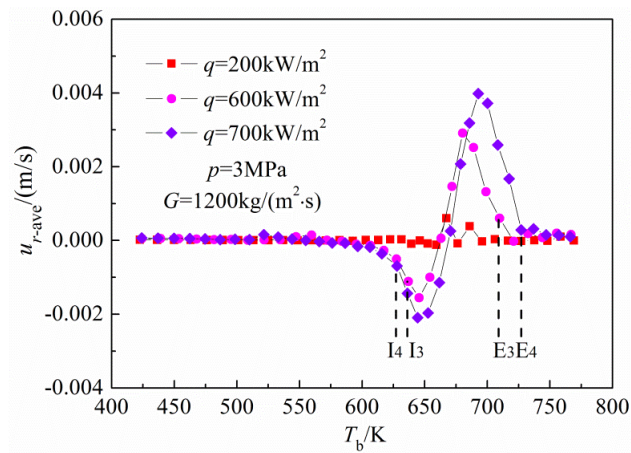


Figure 13 shows the radial velocity distributions in the tube cross-sections corresponding to the deteriorated heat transfer and heat transfer recovered in the high bulk fluid temperature region when the heat flux is 700 kW/m^2 , and the following explanation can be offered for effect mechanism of the radial velocity on heat transfer: firstly, the radial velocity is pointing to the center of tube cross-section, which means that the fluid of cross-section has a trend to flow toward the tube center. Thus, the mixing of hot and cold fluids near the wall is weakened, and the wall cannot be effectively cooled, which resulting in a rapid deterioration of heat transfer along the tube axial direction. Then, the radial velocity begins to change direction to the wall, from the near-wall region gradually extending to the entire radial extent. That is to say, the fluid of the cross-section has a trend to flow toward the wall. As a consequence, the mixing of near-wall fluids is enhanced, and the heat transfer is gradually improved along the flow direction. The demarcation point between the two processes is essentially when the bulk fluid temperature is about the pseudo-critical temperature, but the deterioration and oscillation of turbulent heat transfer in supercritical hydrocarbon fuels, e.g., methane and *n*-heptane, and the radial velocity direction were not necessarily linked in Hua’s study [11,12].

Figure 13. Radial velocity distributions corresponds to the deteriorated heat transfer and heat transfer recovered processes in the high bulk fluid temperature region under a heat flux of 700 kW/m^2 .

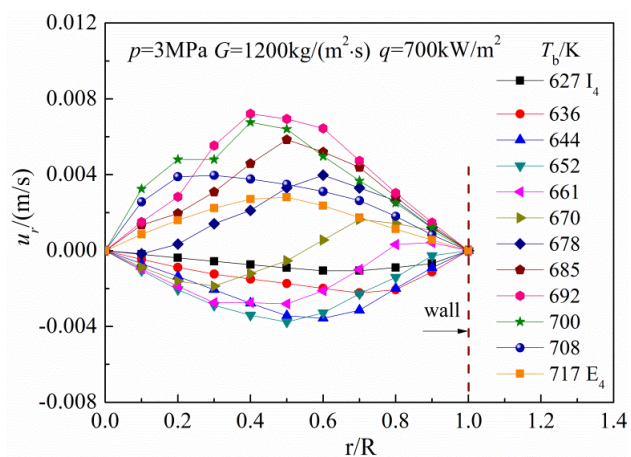
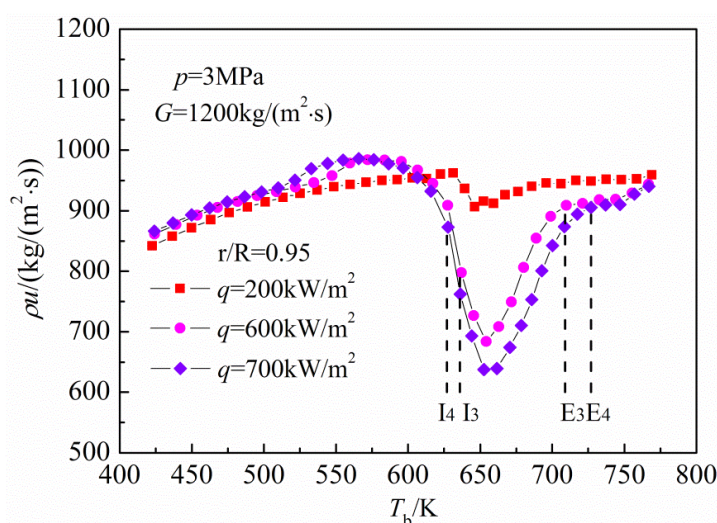


Figure 14 presents the near-wall ($r/R = 0.95$) mass flux variations with bulk fluid temperature under the three heat fluxes. As shown in Figure 14, compared to the operational condition without HTD at low heat flux, the mass flux near the wall shows a significant variation along the tube axial direction, first decreases and then increases corresponding to the deteriorated heat transfer and heat transfer recovered under high heat fluxes. This indicates that abnormal distribution of mass flux appears in the tube cross-sections, the near-wall fluid is brought together to the tube center and leads to an increase of mass flux in the bulk fluid region, while the mass flux in the near-wall region drastically decreases. Obviously, this phenomenon is closely related to the radial velocity oscillation. During the related heat transfer process, *i.e.*, I_i-E_i ($i = 3,4$), as the bulk fluid temperature approaches to the pseudo-critical temperature, the tube cross-section with a larger drastic density variation in its radial direction. Especially in the near-wall region, a large volume of low-density fluid (gas-like) accumulates due to the relatively high fluid temperature.

Figure 14. Variations of the near-wall mass flux with bulk fluid temperature under different heat fluxes.



As a result, the volume and the local pressure of fluid near the wall increases much more than that of the fluid in the bulk fluid region. The pressure imbalance will force the fluid near the wall to the bulk fluid region, so that the wall surface is filmed with a layer of illiquid hot fluid, thus preventing the heat from the wall to the bulk fluid region. This is in fact similar to the film boiling heat transfer under subcritical pressure, and can be considered as a pseudo-film boiling deteriorated heat transfer phenomenon. And then, as the bulk fluid temperature moves away from the pseudo-critical temperature, the pressure imbalance weakens for the reason that the radial fluid density gradient decreases. Therefore, the mass flux near the wall increases owing to the modified radial flow field gradually recovers, and thus the heat transfer is improved along the tube axial direction.

3.3. Critical Condition for the Onset of HTD

The critical condition for the onset of HTD, which is applicable to the *n*-decane at supercritical pressures, is investigated in this section. The pressure range is 3–5 MPa, while the mass flux varies from 400 to 2000 $\text{kg}/(\text{m}^2 \cdot \text{s})$.

The previous studies of deterioration phenomena in heat transfer to supercritical fluids indicated that: at a certain inlet temperature, the onset of HTD depends on the combined effects of pressure, mass flux and heat flux [9,15,16,30,31]. For supercritical inorganic substances, such as water and carbon dioxide, Yamagata *et al.* [30], Styrikovich *et al.* [31], Kim *et al.* [9] developed respectively a series of corrections for critical heat flux of HTD, and concluded that it was only related to the mass flux. However, the related studies for organic substances, including the methane [15] and pentane [16], have also been conducted by Urbano *et al.* [15] and Zhou *et al.* [16], both of which further considered the effect of pressure. The details of these empirical expressions are in Table 2.

Table 2. Selected empirical correlations for critical heat flux of HTD of supercritical fluids.

Author	Correlation	Fluid
Yamagata <i>et al.</i> [30]	$q_{cr} = 0.2 G^{1.2}$	H ₂ O
Styrikovich <i>et al.</i> [31]	$q_{cr} = 0.58 G$	H ₂ O
Kim <i>et al.</i> [9]	$q_{cr} = 0.0002 G^2$	CO ₂
Urbano <i>et al.</i> [15]	$q_{cr} = (0.0432p + 0.0314)G$	CH ₄
Zhou <i>et al.</i> [16]	$q_{cr} = 0.0000855 G^2 + 0.1368 G_p + 4.1 p^2 - 0.162 G + 37p - 42.6$	C ₅ H ₁₂

Figure 15 shows a comparison of the critical heat flux of HTD from the numerical calculations and the empirical expressions at the three different pressures. As shown in Figure 15, none of these empirical expressions are longer valid for the critical heat flux predictions of *n*-decane at supercritical pressures, which may be caused by the differences in fluid properties and operational parameters. It should be noted that the HTD onset is not clearly defined in the literatures [9,16,30,31]. Urbano *et al.* [15] established the following criterion: $(q/G)_{cr}$ appears when $\min(dT_w/dx) = 0$ is satisfied, which is used in the present study. Meanwhile, under the same pressure, a linear relation is found between the critical heat flux and mass flux. When the pressure is 3 MPa, a corresponding critical condition for the onset of HTD is $(q/G)_{cr} = 0.268$ kJ/kg. The heat transfer will be improved with the increasing pressure, hence, under the pressures of 4 and 5 MPa, the corresponding critical conditions for the onset of HTD are increased to $(q/G)_{cr} = 0.493$ kJ/kg and $(q/G)_{cr} = 0.718$ kJ/kg, respectively. Figure 16 further presents variation of $(q/G)_{cr}$ with the pressure. Note that $(q/G)_{cr}$ is also a linear function of the pressure, *i.e.*, $(q/G)_{cr} = 0.225p - 0.407$.

Figure 15. Comparisons of the critical heat flux from the present numerical calculations and the empirical expressions.

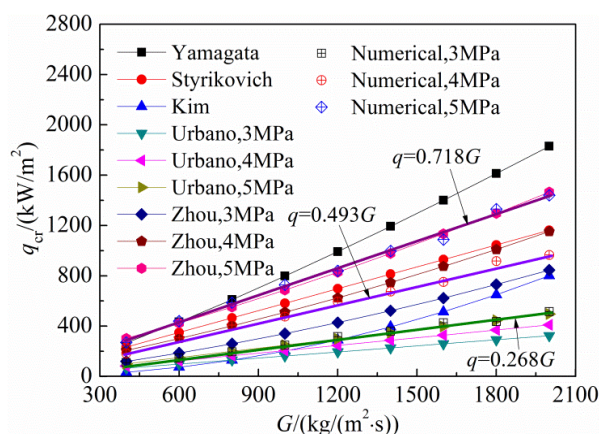
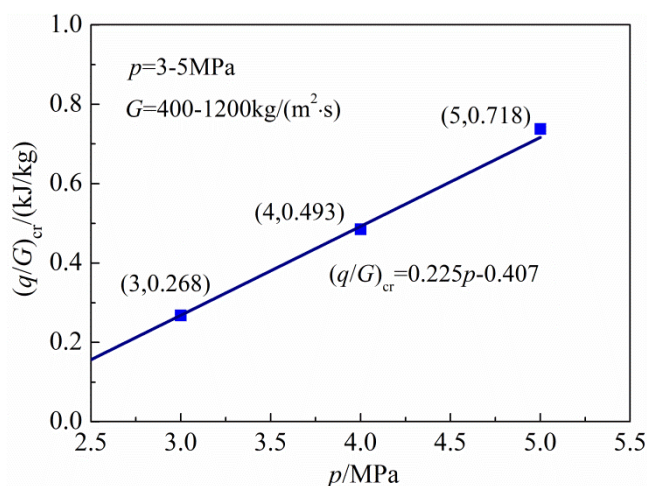


Figure 16. Critical value as a function of the pressure.

Based on the analysis above, a correction for critical heat flux of HTD of *n*-decane at supercritical pressures is developed as follows:

$$q_{cr} = (0.225p - 0.407)G \quad (12)$$

The application range of this expression is that: $1 \leq p/p_c \leq 2.369$, $400 \text{ kg}/(\text{m}^2 \cdot \text{s}) \leq G \leq 2000 \text{ kg}/(\text{m}^2 \cdot \text{s})$. Within this range, the relative error between the calculated values and numerical results is within 4.12%. For a given pressure and mass flux, the HTD will occur when the heat flux is higher than the critical heat flux obtained from this expression.

4. Conclusions

In this paper, a thorough numerical study of the supercritical convective heat transfer of *n*-decane in horizontal circular tubes has been conducted, based on a complete set of conservation equations of mass, momentum and energy, and the RNG k - ϵ turbulence model with enhanced wall treatment. The present numerical study mainly focuses on the fundamental understanding of the HTD phenomena, including the mechanism of HTD, critical condition for the onset of HTD and applicability of empirical heat transfer correlation for HTD, and so on. The following important conclusions could be reached:

- (1) Two different types of HTD phenomena could occur when the wall temperature exceeds the corresponding pseudo-critical temperature under the composite operational conditions of low pressure and high heat flux. Increasing the pressure would effectively alleviate and eliminate the HTDs. The Bae-Kim expression which has higher prediction accuracy when the HTD occurs can be better used for convective heat transfer predictions of *n*-decane at supercritical pressures.
- (2) The onset of HTD occurs because of the drastic density variations in the near-wall and bulk fluid regions, respectively. The HTD with low bulk fluid temperature occurs when the wall temperature is slightly higher than the pseudo-critical temperature, which is caused by the fluid acceleration. The near-wall flow is laminarized and the wall shear stress significantly decreases during the related heat transfer process. The HTD with relatively high bulk fluid temperature

occurs in the large specific heat capacity region, mainly due to the pressure imbalance. During the corresponding heat transfer process, the pressure imbalance leads to the radial velocity oscillation, further affects the mixing ability of near-wall fluids, and the wall surface is filmed with a layer of illiquid hot fluid, thus it can be considered as a pseudo-film boiling deteriorated heat transfer phenomenon.

- (3) Based on the numerical analysis, a new correction for critical heat flux of HTD, which is applicable to the supercritical *n*-decane, has been successfully developed.

Author Contributions

All authors contributed to the work in this manuscript. Yanhong Wang conducted all the analysis and wrote this manuscript. Sufen Li and Ming Dong reviewed and revised the manuscript style. All authors read and approved the final manuscript.

Conflicts of Interest

The authors declare no conflict of interest.

References

1. Huang, H.; Spadaccini, L.J.; Sobel, D.R. Fuel-cooled thermal management for advanced aero-engines. *J. Eng. Gas Turbines Power* **2004**, *126*, 284–293.
2. Sobel, D.R.; Spadaccini, L.J. Hydrocarbon fuel cooling technologies for advanced propulsion. *J. Eng. Gas Turbines Power* **1997**, *119*, 344–351.
3. Zhong, F.Q.; Fan, X.J.; Yu, G.; Li, J.G. Heat transfer of aviation kerosene at supercritical conditions. *J. Thermophys. Heat Transf.* **2009**, *23*, 543–550.
4. Duffey, R.B.; Pioro, I.L. Experimental heat transfer of supercritical carbon dioxide flowing inside channels (survey). *Nucl. Eng. Des.* **2005**, *235*, 913–924.
5. Pioro, I.L.; Duffey, R.B. Experimental heat transfer in supercritical water flowing inside channels (survey). *Nucl. Eng. Des.* **2005**, *235*, 2407–2430.
6. Jiang, P.X.; Zhang, Y.; Zhao, C.R.; Shi, R.F. Convection heat transfer of CO₂ at supercritical pressures in a vertical mini tube at relatively low Reynolds numbers. *Exp. Therm. Fluid Sci.* **2008**, *32*, 1628–1637.
7. Wen, Q.L.; Gu, H.Y. Numerical simulation of heat transfer deterioration phenomenon in supercritical water through vertical tube. *Ann. Nucl. Energy* **2010**, *37*, 1272–1280.
8. Koshizuka, S.; Takano, N.; Oka, Y. Numerical analysis of deterioration phenomena in heat transfer to supercritical water. *Int. J. Heat Mass Transf.* **1995**, *38*, 3077–3084.
9. Kim, J.K.; Jeon, H.K.; Lee, J.S. Wall temperature measurement and heat transfer correlation of turbulent supercritical carbon dioxide flow in vertical circular/non-circular tubes. *Nucl. Eng. Des.* **2007**, *237*, 1795–1802.
10. Zhang, G.; Zhang, H.; Gu, H.Y.; Yang, Y.H.; Cheng, X. Experimental and numerical investigation of turbulent convective heat transfer deterioration of supercritical water in vertical tube. *Nucl. Eng. Des.* **2012**, *248*, 226–237.

11. Wang, Y.Z.; Hua, Y.X.; Meng, H. Numerical studies of supercritical turbulent convective heat transfer of cryogenic-propellant methane. *J. Thermophys. Heat Transf.* **2010**, *24*, 490–500.
12. Hua, Y.X.; Wang, Y.Z.; Meng, H. A numerical study of supercritical forced convective heat transfer of *n*-heptane inside a horizontal miniature tube. *J. Supercrit. Fluids* **2010**, *52*, 36–46.
13. Pizzarelli, M.; Urbano, A.; Nasuti, F. Numerical analysis of deterioration in heat transfer to near-critical rocket propellants. *Numer. Heat Transf. A Appl.* **2010**, *57*, 297–314.
14. Urbano, A.; Nasuti, F. Parametric analysis of heat transfer to supercritical-pressure methane. *J. Thermophys. Heat Transf.* **2012**, *26*, 450–463.
15. Urbano, A.; Nasuti, F. Onset of heat transfer deterioration in supercritical methane flow channels. *J. Thermophys. Heat Transf.* **2013**, *27*, 298–308.
16. Zhou, W.X.; Bao, W.; Qin, J. Deterioration in heat transfer of endothermal hydrocarbon fuel. *J. Therm. Sci.* **2011**, *20*, 173–180.
17. Hitch, B.; Karpuk, M. Enhancement of heat transfer and elimination of flow oscillations in supercritical fuels. In Proceedings of the 34th AIAA/ASME/SAE/ASEE Joint Propulsion Conference and Exhibit, Cleveland, OH, USA, 13–15 July 1998; AIAA98-3759.
18. Liu, Z.H.; Bi, Q.C.; Guo, Y.; Yan, J.G.; Yang, Z.Q. Convective heat transfer and pressure drop characteristics of near-critical-pressure hydrocarbon fuel in a mini-channel. *Appl. Therm. Eng.* **2013**, *51*, 1047–1054.
19. Zhang, L.; Zhang, R.L.; Xiao, S.D.; Jiang, J.; Le, J.L. Experimental investigation on heat transfer correlations of *n*-decane under supercritical pressure. *Int. J. Heat Mass Transf.* **2013**, *64*, 393–400.
20. Dang, G.X.; Zhong, F.Q.; Chen, L.H.; Cheng, X.Y. Numerical investigation on flow and convective heat transfer of aviation kerosene at supercritical conditions. *Sci. China-Technol. Sci.* **2013**, *56*, 416–422.
21. Liu, B.; Wang, X.; Zhu, Y.H.; Jiang, P.X. Experimental investigation of convective heat transfer of *n*-decane at supercritical pressures in a micro/mini vertical tube. *J. Eng. Thermophys.* **2014**, *35*, 114–118.
22. Shiralkar, B.S.; Griffith, P. Deterioration in heat transfer to fluids at supercritical pressure and high heat fluxes. *J. Heat Transf.* **1969**, *91*, 27–36.
23. Ruan, B.; Meng, H.; Yang, V. Simplification of pyrolytic reaction mechanism and turbulent heat transfer of *n*-decane at supercritical pressures. *Int. J. Heat Mass Transf.* **2014**, *69*, 455–463.
24. Bae, Y.Y.; Kim, H.Y. Convective heat transfer to CO₂ at a supercritical pressure flowing vertically upward in tubes and an annular channel. *Exp. Therm. Fluid Sci.* **2009**, *33*, 329–339.
25. Linne, D.L.; Meyer, M.L.; Edwards, T.; Eitman, D.A. Evaluation of heat transfer and thermal stability of supercritical JP-7 fuel. In Proceedings of the 33rd AIAA/ASME/SAE/ASEE Joint Propulsion Conference and Exhibit, Seattle, WA, USA, 6–9 July 1997; AIAA97-3041.
26. Cheng, X.; Kuang, B.; Yang, Y.H. Numerical analysis of heat transfer in supercritical water cooled flow channels. *Nucl. Eng. Des.* **2007**, *237*, 240–252.
27. Urbano, A.; Pizzarelli, M.; Nasuti, F. Numerical analysis of transcritical fluids heating in liquid rocket engine cooling channels. *J. Aerosp. Sci.* **2009**, *88*, 20–30.
28. Giovanetti, A.J.; Spadaccini, L.J.; Szetela, E.J. Deposit formation and heat transfer characteristics of hydrocarbon rocket fuels. *J. Spacecr. Rockets* **1985**, *22*, 574–580.

29. McEligot, D.M.; Jackson, J.D. “Deterioration” criteria for convective heat transfer in non-circular ducts. *Nucl. Eng. Des.* **2004**, *232*, 327–333.
30. Yamagata, K.; Nishikawa, K.; Hasegawa, S.; Fujii, T.; Yoshida, S. Forced convective heat transfer to supercritical water flowing in tubes. *Int. J. Heat Mass Transf.* **1972**, *15*, 2575–2593.
31. Styrikovich, M.A.; Margulova, T.K.; Miropolskiy, Z.L. Problem in the development of designs of supercritical boilers. *Teploenergetika* **1967**, *14*, 4–7.

© 2014 by the authors; licensee MDPI, Basel, Switzerland. This article is an open access article distributed under the terms and conditions of the Creative Commons Attribution license (<http://creativecommons.org/licenses/by/4.0/>).